IFUSP/P-63

TETRAHEDRAL ANTIFERROMAGNETISM IN $Ni(BrO_3)_2 6H_2O$ *

by

N.F. Oliveira Jr. and S. Frota-Pessôa

Instituto de Física, Universidade de São Paulo ,
C.P. 20516, São Paulo, Brazil.

* Work partially supported by CNPq and FINEP.

Submitted for publication in SOLID STATE COMMUNICATIONS.

TETRAHEDRAL ANTIFERROMAGNETISM IN $Ni(BrO_3)_2 6H_2O$*

by

N.F. Oliveira Jr. and S. Frota-Pessôa

Instituto de Física, Universidade de São Paulo, C.P. 20516

São Paulo - Brasil

ABSTRACT

The magnetic susceptibility of $Ni(BrO_3)_2 6H_2O$ was measured from 20 K down to 0.07 K . A sharp peak at 0.21 K is interpreted as the onset of longe range antiferromagnetic order of the tetrahedral type.

* Work partially supported by CNPq and FINEP

Among the possible spin arrangements for an fcc lattice predicted by molecular field theories of antiferromagnetism, there is one which has not yet been observed. It is the tetrahedral arrangement[1]. In this configuration, the fcc lattice is divided into four sublattices with each sublattice magnetization aligning in the direction of one of the cube diagonals, and with the total magnetization being zero. It is the purpose of this paper to present evidence that this type of arrangement occurs in $Ni(BrO_3)_2 6H_2O$.

This salt is isomorphous to the $Zn(BrO_3)_2 6H_2O$ whose crystalline structure has been investigated in detail[2]. The Ni^{++} ions form an fcc lattice with the six water molecules surrounding the Ni^{++} and forming a distorted octahedron. This distortion is such that it maintains a three-fold axis coincident with the cube diagonal, and each of the four $Ni6H_2O^{++}$ complexes of the unit cell has its symmetry axis along a different cube diagonal. So, it is reasonable to suppose that the crystalline field acting on each Ni^{++} ion has axial symmetry in such a way to favor the antiferromagnetic arrangement of the tetrahedral type. In fact, ESR studies in this salt were interpreted in these terms, yielding a splitting of the Ni^{++} ground spin triplet of $(|D| / k) \simeq 2$ K and $(E/k) \simeq 0$ K , at 4.2 K[3].

We have performed zero-field magnetic susceptibility measurements on powdered samples of $Ni(BrO_3)_2 6H_2O$, at H_2 , He^4 and He^3 temperatures. The experimental apparatus used has been described previously[4]. These measurements, as shown in Fig. 1, exhibit a Curie-Weiss behavior with small deviations

only between 0.5 K and 2.5 K . A least-square fit of the data between 14 K and 20 K yields a g-factor of 2.25 ± 0.01 (assuming S = 1), and a Weiss temperature of $\theta = -0.5 \pm 0.1$ K . This value of θ suggests that an antiferromagnetic interaction is present between the Ni^{++} spins, which could result in long range order at very low temperatures, provided that the sign of the parameter D (not revealed by the ESR) was such that the almost degenerate doublet, $|+1>$ and $|-1>$, lies lower in energy.

With that in mind we have built a small adiabatic demagnetization refrigerator to cool a powdered sample of $Ni(BrO_3)_2 6H_2O$ below 0.1 K . Since here the sample could not be removed from the pick-up coil, only variations of the susceptibility χ were measured. To obtain absolute values of χ , a fit of the variation observed in the interval 4.2 K to 1.2 K was made to the absolute values previously obtained at the same temperature. Fig. 2 shows all the data obtained below 1.5 K . Two features are prominent: the sharp peak at 0.21 K and the sudden decrease below this temperature.

To test our hypothesis of tetrahedral antiferromagnetism, we have calculated the zero field susceptibility $\chi(T)$ for this configuration in the molecular field approximation (MFA), including second neighbor interactions. Following Smart[1] , we divided each of the four simple cubic sublattice into two face centered ones, so that there is interaction only between spins of different sublattices, and took $\vec{M}_1 = \vec{M}_5$, $\vec{M}_2 = \vec{M}_6$, $\vec{M}_3 = \vec{M}_7$, and $\vec{M}_4 = \vec{M}_8$. With this subdivision, a given spin has two of its nearest neighbors on each of the six other sublattices and its

six second nearest neighbors on the remaining one. For simplicity we assumed the test field $\delta\vec{H}$ directed along one of the cube edges, and it is easy to see that this gives also the powder susceptibility. Fig. 3 gives a schematic view of the sublattice magnetizations and the axes involved in the calculation. From symmetry arguments we assumed the variations in the sublattice magnetizations, $\delta\vec{M}_i$, due to the test field $\delta\vec{H}$, to have components parallel $(\delta\vec{M}_{//})$ and perpendicular $(\delta\vec{M}_{\perp})$ to $\delta\vec{H}$ which are of the same magnitude for all sublattices. The perpendicular components cancel each other so that $\chi(T)$ is given by $8\ \delta M_{//}(T) / \delta H$. To obtain $\delta M_{//}(T) / \delta H$ we calculated the magnetization of sublattice 1 in the reference system x , y , z as defined in Fig. 3 (the x-axis is perpendicular to the plane of the figure). The one-ion Hamiltonian was then assumed

$$H = D\, S_{1z}^2 + g\, \mu_B\, (S_{1z}\, H_{1z}^e + S_{1y}\, H_{1y}^e) \quad , \tag{1}$$

where μ_B is the Bohr magneton, and H_{1z}^e and H_{1y}^e are the z and y components of the effective field acting on the first sublattice. This effective field could be written as

$$\vec{H}_1^e = \delta\vec{H} - (2\gamma - \gamma')\, \vec{M}_1^o + 2\gamma\, (\delta\vec{M}_2 + \delta\vec{M}_3 + \delta\vec{M}_4) + \gamma'\, \delta\vec{M}_1 \tag{2}$$

where γ and γ' are related to the exchange parameters for nearest (J_1) and next-nearest (J_2) neighbor interactions by $\gamma = .32\ J_1 / Ng^2\, \mu_B{}^2$ and $\gamma' = 96\ J_2 / Ng^2\, \mu_B{}^2$. $\vec{M}_i^o$ is the magnetization of sublattice 1 for $\delta\vec{H} = 0$ and N is the total number of spins. Treating the last term of Eq.1 as a perturbation

and correcting the energies up to second order and the eigenstates up to first order, we calculated the mean values of S_z and S_y. After some manipulation we obtained:

$$M_1^o = \frac{Ng\,\mu_B}{8} \frac{2\ \mathrm{senh}\ (\alpha M_1^o / kT)}{\exp(D/kT) + 2\cosh\ (\alpha M_1^o / kT)} \tag{3}$$

where $\alpha = -g\,\mu_B\,(2\gamma - \gamma') > 0$.

$$\chi^{-1}(T) = \frac{\left[1 - (6\gamma+\gamma')\ A\right]\left[(2\gamma-\gamma')\ B + 1\right]\cos^2\phi}{8\left\{\left[(2\gamma-\gamma')\ B+1\right] A\cos^2\phi + B\,\mathrm{sen}^2\phi\left[(2\gamma-\gamma')\ A+1\right]\right\}} +$$

$$+ \frac{\left[1 - (6\gamma-\gamma')\ B\right]\left[(2\gamma-\gamma')\ A + 1\right]\mathrm{sen}^2\phi}{8\left\{\left[(2\gamma-\gamma')\ B+1\right] A\cos^2\phi + B\,\mathrm{sen}^2\phi\left[(2\gamma-\gamma')\ A+1\right]\right\}} \tag{4}$$

where

$$A = \frac{N}{4}\frac{g^2\mu_B{}^2}{kT}\left\{\frac{\exp(D/kT)\cosh\ (\alpha M_1^o/kT) + 2}{\left[\exp(D/kT) + 2\cosh\ (\alpha M_1^o/kT)\right]^2}\right\}$$

$$B = \frac{N}{8}\frac{g^2\mu_B{}^2}{kT}\left\{\frac{(e^b - 1)/b + (e^a - 1)/a}{1 + e^a + e^b}\right\}$$

$$a = (-D + \alpha M_1^o)/kT \quad \text{and} \quad b = (-D - \alpha M_1^o)/kT\ .$$

The condition for Eq.(3) to have a small non vanishing solution yields:

$$T_N = \frac{Ng^2\mu_B{}^2}{4k}\frac{(\gamma' - 2\gamma)}{\exp(D/kT_N) + 2}\ . \tag{5}$$

and the behavior of Eq.(4) at high temperatures ($T >> |D/k|, T_N$) gives:

$$\theta = \frac{Ng^2\mu_B^2}{12k}(6\gamma + \gamma') \qquad (6)$$

Using the values $\theta = -0.5$, $g = 2.25$ and $T_N = 0.21$ K we tried to fit the low temperature data by the above equations taking D as an adjustable parameter. A good fit was possible only if D is negative (doublet lying lower) and much larger than T_N . The solid line in Fig. 2 corresponds to $(D/k) = -2$ K and the agreement with the experimental points is remarkable. Somewhat larger values of $|D|$ would not change appreciably the paramagnetic part of the curve, but would decrease the value of $\chi(0)$. The experimental points do not go low enough in temperature to determine $\chi(0)$, but they stablish the lower limit of ~ 1.8 K for $|D|$. This is in agreement with the ESR data[3].

From equations (5) and (6) and using the experimental values of θ and T_N we obtain $J_1 = -0.03\ ^oK$ and J_2 about 12 times smaller both being antiferromagnetic. It should be noted here, however, that the next nearest neighbor interaction was included only to make possible a complete interpretation of the data in terms of the MFA , since otherwise the observed ratio θ / T_N could not be explained. It is well known, however, that θ / T_N may be highly influenced by spin fluctuation effects and so the value of J_2 must be taken with reserve.

In conclusion, the present measurements indicate that below 0.21 K the salt $Ni(BrO_3)_2 6H_2O$ exhibits long range

antiferromagnetic order of the tetrahedral type, for the Ni^{++} spins. This is, to our knowledge, the first material for which there exists strong evidence of this type of antiferromagnetic ordering.

We would like to thank Dr. H. Vargas and Mr. J. Suassuna for making their preliminary experimental value of $|D|$ and E available to us.

REFERENCES

(1) SMART, J.S., Effective Field Theories of Magnetism (W.B. Saunders, Philadelphia, 1966) p. 75.

(2) YU, S.H. and BEEVERS, C.A., Z. Krist. 95, 426 (1936).

(3) SUASSUNA, J. and VARGAS, H., to be published.

(4) OLIVEIRA JR, N.J. and QUADROS, C.J., J. Phys. E : Sci. Instr. 2 967 (1969).

FIGURE CAPTIONS

Fig. 1 - Inverse of the molar susceptibility versus temperature. Dashed line corresponds to the best fit of the data between 14 K and 20 K .

Fig. 2 - Molar susceptibility versus temperature. Data from two independent adiabatic demagnetization runs are shown. The bars shown in two experimental points indicate the tipical estimated uncertainty for the points below 0.3 K . The solid line is the calculated curve for $g = 2.25$, $\theta = -0.5$ K and $D/k = -2$ K .

Fig. 3 - Schematic diagram of the sublattice magnetizations. The vectors corresponding to $\vec{M}_3^o = \vec{M}_7^o$ and $\vec{M}_4 = \vec{M}_8$ lie in the plane perpendicular to the figure, which constains $\delta\vec{H}$, that is, the dashed vectors should be viewed rotated by 90^o about the axis of $\delta\vec{H}$.

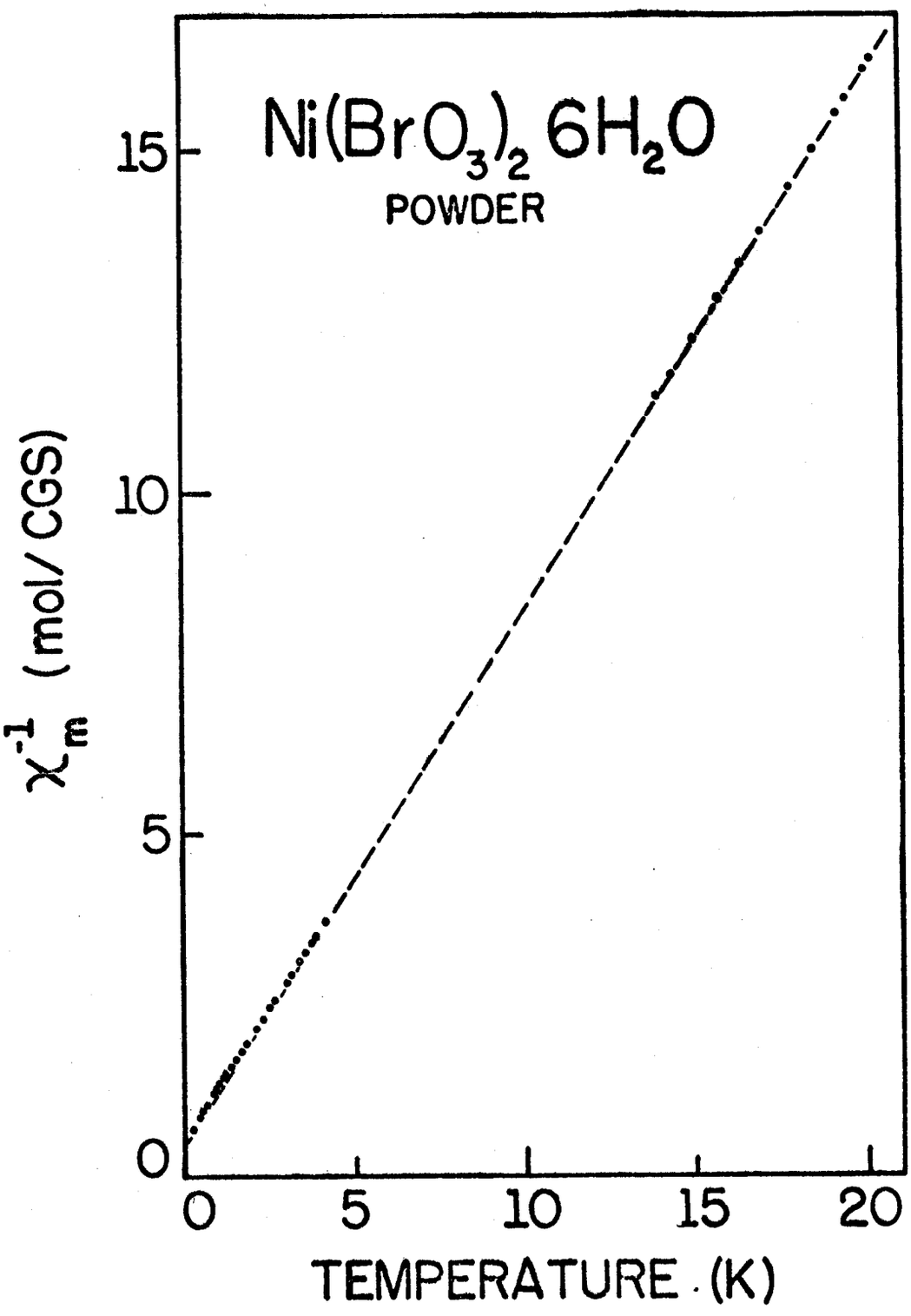
Ni(BrO3)2 6H2O
POWDER
15
10
5
0
χ-1m (mol/CGS)
0
5
10
15
20
TEMPERATURE (K)

Fig. 1

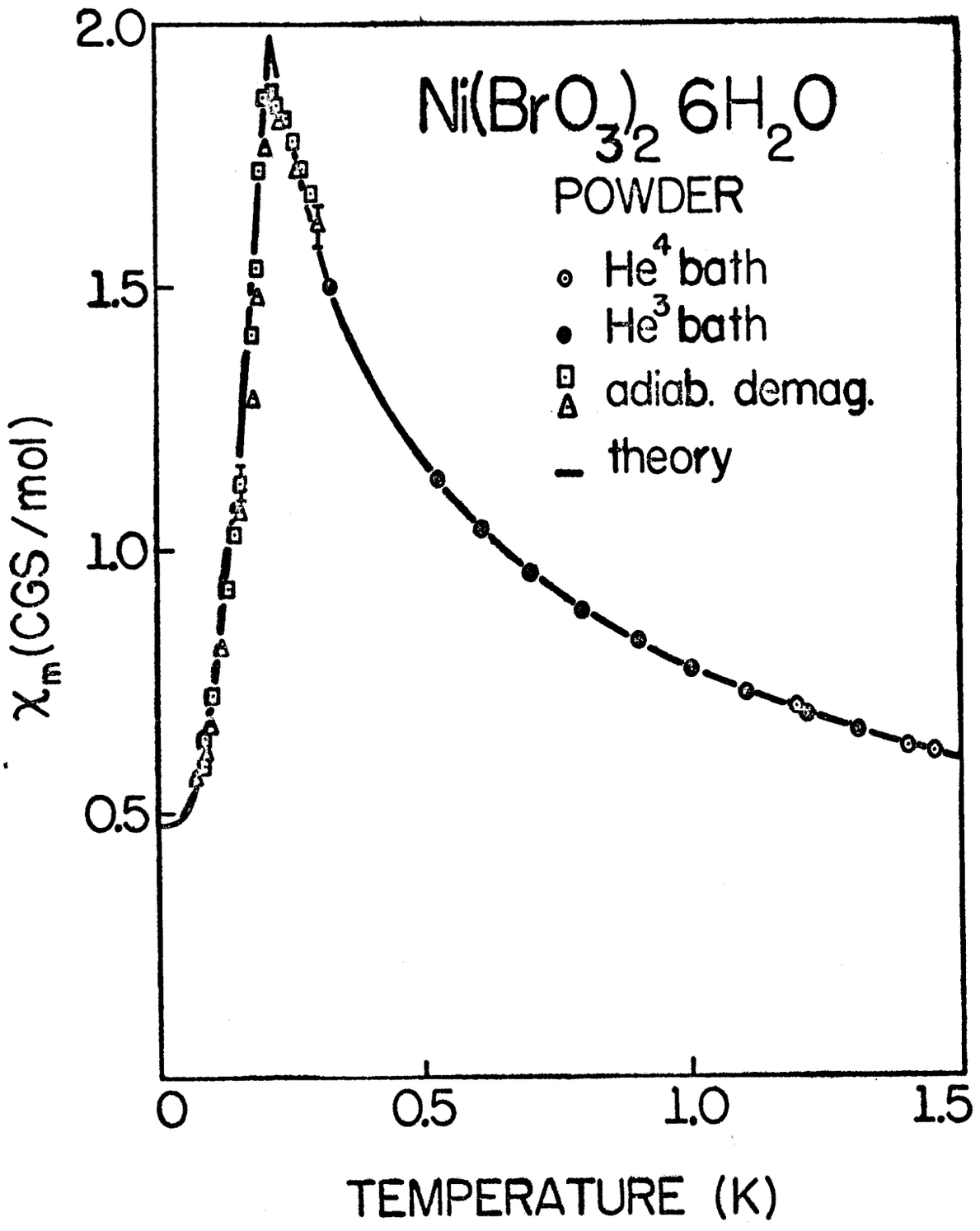
2.0
1.5
1.0
0.5
χ_m (CGS/mol)
$Ni(BrO_3)_2\,6H_2O$
POWDER
He^4 bath
He^3 bath
adiab. demag.
theory
0
0.5
1.0
1.5
TEMPERATURE (K)

Fig. 2

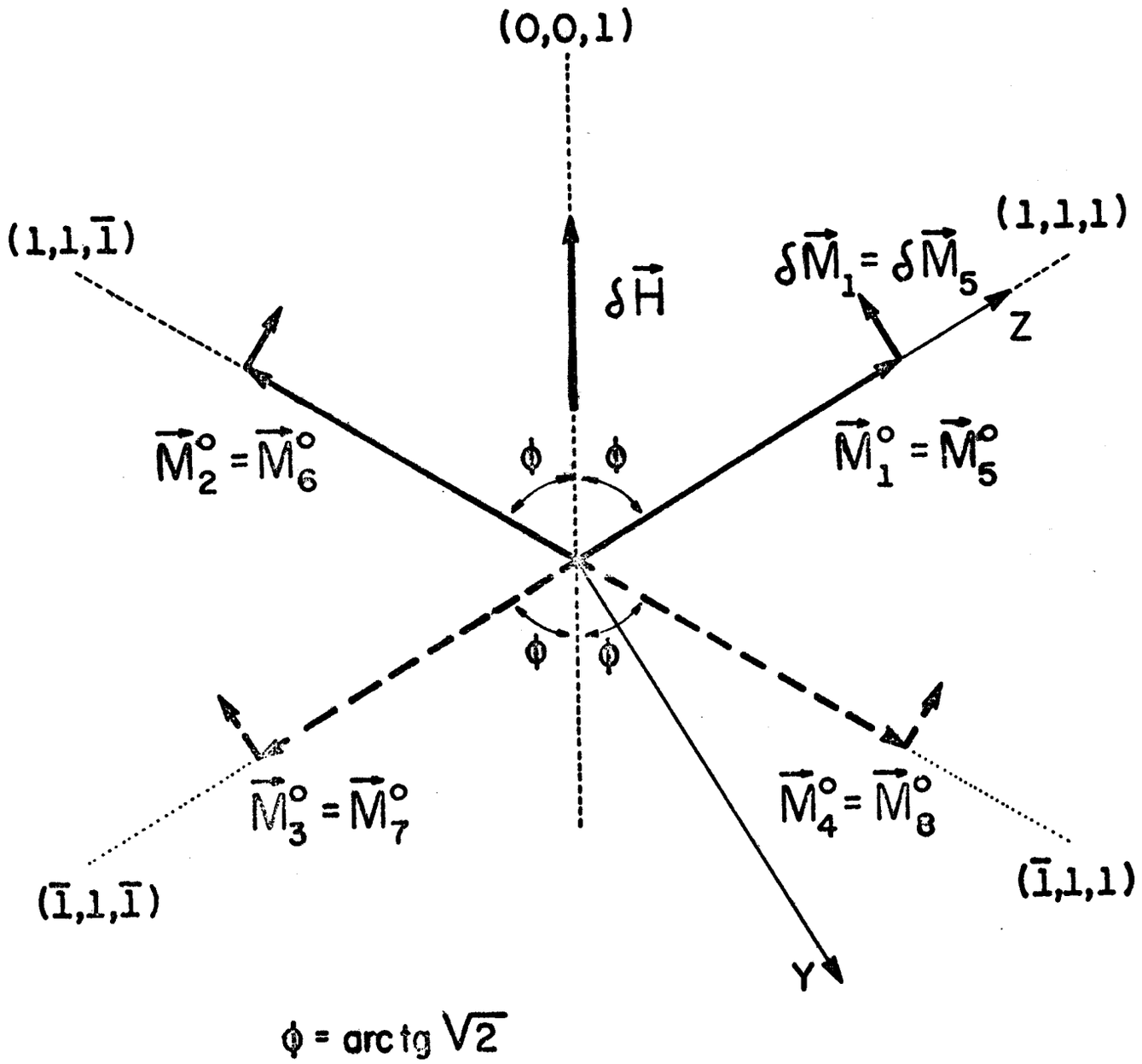
(0,0,1)
(1,1,$\bar{1}$)
(1,1,1)
$\delta\vec{H}$
$\delta\vec{M}_1 = \delta\vec{M}_5$
Z
$\vec{M}_2^\circ = \vec{M}_6^\circ$
$\vec{M}_1^\circ = \vec{M}_5^\circ$
ϕ
ϕ
ϕ
ϕ
$\vec{M}_3^\circ = \vec{M}_7^\circ$
$\vec{M}_4^\circ = \vec{M}_8^\circ$
($\bar{1}$,1,$\bar{1}$)
($\bar{1}$,1,1)
Y
ϕ = arc tg $\sqrt{2}$

Fig. 3